



Application of Auxetic Core to Improve Dynamic Response of Sandwich Panels Under Low-Velocity Impact

Hasan Biglari¹ · Hadi Teymouri¹ · Mohammad Foroutan¹

Received: 31 July 2023 / Accepted: 28 January 2024 / Published online: 10 March 2024
© King Fahd University of Petroleum & Minerals 2024

Abstract

Using high-order shear and normal deformation theory (HSNDT), this study analyzes the dynamic response and time history of the impact force of the sandwich plate with the auxetic core under low-velocity impact. The impact was modeled using a two-degree-of-freedom mass and spring model, and the Hertz linearized model was utilized to derive the contact force's time history. The rectangular sandwich panel has simple supported boundary conditions and consists of three layers: two aluminum top face sheets and one auxetic core layer with a negative Poisson's ratio. Using the energy technique, the system's governing equations are derived. The equilibrium equations were solved by the analytic approach of the Navier method in the space domain and the numerical method of Newmark in the time domain. The use of HSNDT distinguishes this article from others on similar topics, and the flexibility of the thick core in the thickness direction is considered. The Effects of different geometric and material properties have been investigated, and the results have been compared with those of other similar papers and studies for validation. The data indicate that the greater the degree of inclination of the cell, the longer the impact period and the lower the peak impact force. Moreover, the larger angle of the auxetic cell reduces the deflection at the impact site. In terms of minimizing deflection, the auxetic honeycomb sandwich panel is 25% superior to the non-auxetic honeycomb panel.

Keywords Low-velocity impact · Higher-order shear and normal deformation theory · Auxetic material · Mass-spring model · Sandwich panel

1 Introduction

Due to the extensive usage of sandwich panels in the production of various structures, it is crucial to understand their mechanical characteristics. In the majority of instances, sandwich panel face sheets can bear in-plane normal (bending) stresses, while the core can withstand shear and transverse normal stresses. The core is the most crucial component of sandwich construction. The core material should have qualities such as low density to reduce the weight of the structure, a high vertical Young's modulus to avoid excessive deformation along the thickness, and a quick decrease in bending stiffness [1]. Sandwich panels are susceptible to impact damage due to the lack of a reinforcing component in the thickness direction. Typically, sandwich panels are

subject to impacts from exterior components such as bird and stone strikes. Low-velocity impact damage is crucial in aerospace applications because, although it is undetectable during standard inspections, it may reduce the compressive strength of sandwich panels by 30 to 40 percent [2]. The impact often causes warping, cracking of the matrix, and breaking of the fibers in the tops, as well as core failure and separation of the top from the core [3].

The law of impact, which links the equations of motion of the impacting objects, describes the connection between the indentation and the collision force [4]. Hertz [5] conducted the first study on the subject of the law of static impact; he examined the issue of the impact between two homogeneous isotropic elastic masses. Sveklo's impact law is another considered impact law. This impact rule is also known as the Hertz–Sveklo theory due to the many similarities between Sveklo's method for the issue of contact loading of non-isotropic substances and Hertz's theory in many respects (Mittal & Khalili [6]). The low-velocity impact reactions and crashworthiness of various aluminum foam-core sandwich

✉ Hasan Biglari
hbiglari@tabrizu.ac.ir

¹ Department of Mechanical Engineering, University of Tabriz, Tabriz, Iran



constructions were examined by Huo et al. [7]. Guo et al. [8] have carried out thorough examinations on sandwich structures subjected to different impact loads.

There are several mathematical approaches for simulating impact, including the energy balance model and the mass and spring model. Lal [9] introduced a mass and spring design with two degrees of freedom, where the second degree of freedom added to the preceding design is the impactor's stiffness. He analyzed the sheet's bending, shearing, and collision stiffnesses. Khalili [10] examined the orthotropic sheet subjected to impact stress. He employed the Hertz–Svejklo hypothesis for the impact, assuming that the sheet was infinitely big. He also used classical sheet theory and Fourier transformations to get the dynamic response of the sheet analytically. Malekzadeh et al. [11, 12] employed innovative mass-spring-damper vibration designs with three degrees of freedom to calculate and derive the dynamic response of a sandwich sheet by considering transverse flexibility and structural damping. Bagheri et al. [13, 14] conducted a study where they examined the response of sandwich structures with a polypropylene core reinforced with nanoparticles to low-velocity impacts. The investigation involved both experimental and numerical methods.

Due to their exceptional mechanical qualities, which include low mass, high specific stiffness or strength, outstanding energy absorption capacity, and other multifunctional qualities, lightweight metallic cellular materials (MCMs) have been used in many technical applications to date [15, 16]. Materials having a negative Poisson ratio have drawn the attention of academics in recent years as one of these novel situations. This indicates that, owing to axial stress, their transverse length increases [17]. Lakes [18] transformed a regular material into an auxetic for the first time by employing heating, cooling, condensation, and regeneration time. Based on the huge deviation theory, Wan et al. [19] provided a theoretical technique for calculating Poisson's ratio of honeycomb networks. Zhang et al. [20] examined the influence of auxetic honeycomb cell microstructure on in-plane stochastic behavior and energy absorption using the finite element technique. Huang et al. [21] introduced a novel design for the auxetic honeycomb, including a hexagonal component and a thin plate. Prawoto [22] has explored the mechanical characteristics and applications of auxetic materials. Qin et al. [23] conducted an investigation into novel failure modes when dynamically compressing metal honeycomb-like hierarchical structures featuring perforated walls.

The impact response of sandwich panels has been analyzed using a variety of methods. The first-order shear deformation theory (FSDT) and the higher-order shear deformation theory (HSDT) disregard the transverse flexibility of the core and the interaction between the processes and the flexible core [24, 25]. Zhang et al. [26] conducted an

investigation into the effects of a large mass at low velocity on sandwich beams consisting entirely of an affixed metal foam core and fiber-metal laminate face sheets. Frostig et al. [27] provided a high-order theory (HSAPT) for a sandwich beam with a flexible transverse core based on the laws of change. The longitudinal and lateral changes of the core were determined using the fundamental equations of the isotropic material and compatibility criteria in the common face, as well as nonlinear expressions for the thickness coordinates. By updating Frostig's higher-order theory of sandwich plates, Malekzadeh et al. [28] developed a revised and enhanced higher-order theory of sandwich plates. In this theory, the contribution of the plane forces of the top and lower surfaces of the sandwich sheet and the equivalent consumption factor of the sandwich sheet was estimated, and for the study of vibrations, the damping of the system was also explored. Zhang et al. [29] investigated the effects of a large mass on constrained square sandwich plates (SSP) composed of fiber-metal laminate (FML) face sheets and a metal foam core subjected to low-velocity impact. Additionally, they examined the response of fully clamped multilayer sandwich beams with metal foam cores under low-velocity impact conditions. They employed analytical, experimental, and numerical techniques in their investigation [30].

Yang et al. [31] studied the vertical impact resistance of a sandwich panel with an auxetic core. In their study, a sandwich panel with an aluminum foam core and an auxetic honeycomb was investigated numerically (using a finite element method) and then experimentally (an impact test). Allen et al. [32] did an experimental study on open-cell auxetic foam and regular PU foam subjected to quasi-static and low-velocity impacts. Chang et al. [33] studied experimentally and statistically the impact resistance of sandwich panels with an aluminum shell and an auxetic internal honeycomb core and determined that the auxetic internal honeycomb is more resistant than other forms of auxetic honeycomb. Beharic et al. [34] investigated the amount of energy absorbed by different sandwich panels with auxetic honeycomb cores, including mesh, interior, and truss, during a drop weight impact test. Hou et al. [35] performed an experimental study on the impact resistance of auxetic and non-auxetic composites subjected to low-velocity loads. Multiscale modeling and nonlinear impact analysis of sandwich panels with graphene-reinforced composite faceplates and functionally graded (FG) three-dimensional auxetic lattice cores were reported by Li et al. [36]. Plastic failure modes were measured by Qin et al. [37], who conducted experiments on sandwich plates that were entirely fastened and subjected to low-velocity impact from a drop hammer featuring a hemispherical muzzle.

For the analytical solution of sandwich panels, there are several theories, including first-order and higher-order shear deformation theories, the zigzag theory, the layered theory,

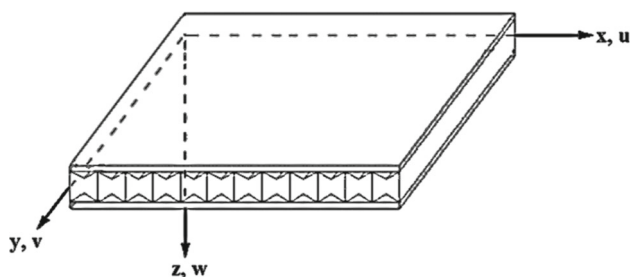


Fig. 1 Schematic of an internal auxetic honeycomb sandwich panel

and the sinusoidal theory, among others [38–40]. Excellent research on sandwich panels under load. Nevertheless, fewer of these investigations have viewed the core as auxetic.

As mentioned, numerous studies have been conducted in the area of low-velocity impacts of sandwich panels with auxetic cores, but fewer of these researches are parametric studies and analytical. In this article, an effort will be made to determine the dynamic response of a low-velocity impact on a sandwich panel with an auxetic core using high-order shear and normal deformation theory (HSNDT) with transverse flexibility along the panel’s thickness. The impact force history is computed using two degrees of freedom of the mass and spring model and the linearized Hertz model.

2 Modeling the System and Getting its Governing Equations

The schematic of the rectangular sandwich panel under investigation is shown in Fig. 1. Cartesian coordinates (x , y , and z) are used to indicate spatial coordinates and displacement components of object points, as seen in this diagram. The proposed sandwich panel is a rectangular sheet with dimensions a and b and a uniform thickness of h and two isotropic surfaces and a soft and flexible auxetic central core. In the dynamic analysis of the sheet, modest displacements are considered, and the linear elastic range is assumed for the analysis. The layers and the central core are integrally linked, and the strain functions are continuous at the connecting surfaces of the layers. The coordinate system is defined so that the x – y plane coincides with the plane in the center. The thickness of the top layer, the middle layer, and the bottom layer are h_t , h_c , and h_b , respectively.

2.1 Auxetic Core

As shown in Fig. 1, the core employed in this sandwich panel is a sort of concave or inward honeycomb auxetic core. Figure 2 depicts the schematic of a core unit cell of the internal auxetic honeycomb and geometric parameters.

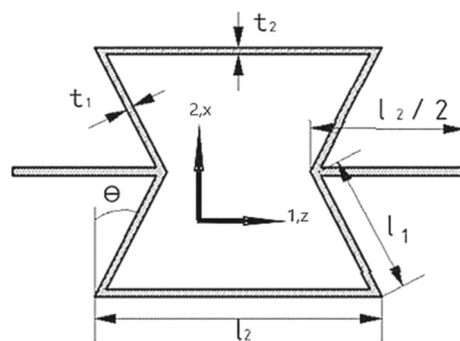


Fig. 2 Schematic representation of the unit cell core of an internal auxetic honeycomb [41]

As shown in the figure, l_1 and l_2 are the lengths of the cellular’s straight and sloping walls, t_1 and t_2 are their thicknesses, and θ is the cellular’s inclined angle.

The equivalent elastic properties of the core layer are determined from the bending and tensile deformations of the core cells using the following formulas [42]:

$$E_1^{(2)} = E_s \frac{\eta_3^3 (\eta_1 - \sin \theta)}{\cos^3 \theta [1 + (\tan^2 \theta + \eta_1 \sec^2 \theta) \eta_3^2]} \tag{1}$$

$$E_2^{(2)} = E_s \frac{\eta_3^3}{\cos \theta (\eta_1 - \sin \theta) (\tan^2 \theta + \eta_3^2)} \tag{2}$$

$$G_{12}^{(2)} = E_s \frac{\eta_3^3}{\eta_1 (1 - 2\eta_1) \cos \theta} \tag{3}$$

$$G_{23}^{(2)} = G_s \frac{\eta_3 \cos \theta}{\eta_1 - \sin \theta} \tag{4}$$

$$G_{31}^{(2)} = \cos \frac{\eta_3}{2 \cos \theta} \left[\frac{\eta_1 - \sin \theta}{1 + 2\eta_1} + \frac{\eta_1 + 2 \sin^2 \theta}{2(\eta_1 - \sin \theta)} \right] \tag{5}$$

$$v_{12}^{(2)} = - \frac{\sin \theta (1 - \eta_3^2) (\eta_1 - \sin \theta)}{\cos^2 \theta [1 + (\tan^2 \theta + \sec^2 \theta \eta_1) \eta_3^2]} \tag{6}$$

$$v_{21}^{(2)} = - \frac{\sin \theta (1 - \eta_3^2)}{(\tan^2 \theta + \eta_3^2) (\eta_1 - \sin \theta)} \tag{7}$$

$$\rho^{(2)} = \rho_s \frac{\eta_3 (\eta_1 + 2)}{2 \cos \theta (\eta_1 - \sin \theta)} \tag{8}$$

where $\eta_1 = \frac{l_2}{l_1}$, $\eta_2 = \frac{t_2}{t_1}$, and $\eta_3 = \frac{h}{l_1}$. In the above relations, superscript 2 indicates that the material properties are related to the second layer (core). In addition, the values of E_s , ρ_s , and G_s correspond to the coefficients of elastic modulus, shear modulus, and density of material that makes up the core.

2.2 HSNDT Displacement Field

To obtain the sandwich panel’s equations of motion, Hamilton’s principle and HSNDT are used, in which deflection in

the direction of the constant thickness is not considered and flexibility of the core in the direction of thickness is considered. So, based on the sandwich panel’s characteristics, HSDNT is a more realistic theory than the other classical theories. This theory divides deflection into three phases: bending, shearing, and thickness stretching. This theory has five unknown general variables, compared to six or more in other shear and normal deformation theories. According to this theory, the displacement field is supposed to be as follows [43]:

$$\begin{aligned}
 u(x, y, z, t) &= u_0(x, y, t) - z \frac{\partial w_b}{\partial x} - f(z) \frac{\partial w_s}{\partial x} \\
 v(x, y, z, t) &= v_0(x, y, t) - z \frac{\partial w_b}{\partial y} - f(z) \frac{\partial w_s}{\partial y} \\
 w(x, y, z, t) &= w_b(x, y, t) + w_s(x, y, t) + g(z)\varphi(x, y, t)
 \end{aligned}
 \tag{9}$$

In the preceding relationship, u_0 and v_0 represent mid-plane displacement along x and y axis, respectively. Also, w_b , w_s and φ are transverse deflection due to bending, shearing, and deformation along the thickness, respectively.

And:

$$\begin{aligned}
 f(z) &= z - h \sinh\left(\frac{z}{h}\right) + z \cosh\left(\frac{1}{2}\right) \\
 g(z) &= \cosh\left(\frac{z}{h}\right) - \cosh\left(\frac{1}{2}\right)
 \end{aligned}
 \tag{10}$$

Sandwich plate strain–displacement relations are given as the following equations:

$$\begin{aligned}
 \begin{Bmatrix} \varepsilon_x \\ \varepsilon_y \\ \gamma_{xy} \end{Bmatrix} &= \begin{Bmatrix} \varepsilon_x^0 \\ \varepsilon_y^0 \\ \gamma_{xy}^0 \end{Bmatrix} + z \begin{Bmatrix} k_x^b \\ k_y^b \\ k_{xy}^b \end{Bmatrix} + f \begin{Bmatrix} k_x^s \\ k_y^s \\ k_{xy}^s \end{Bmatrix}, \begin{Bmatrix} \gamma_{yz} \\ \gamma_{xz} \end{Bmatrix} \\
 &= g \begin{Bmatrix} \gamma_{yz}^0 \\ \gamma_{xz}^0 \end{Bmatrix}, \varepsilon_z = g' \varepsilon_z^0
 \end{aligned}
 \tag{11}$$

where:

$$\begin{aligned}
 \begin{Bmatrix} \varepsilon_x^0 \\ \varepsilon_y^0 \\ \gamma_{xy}^0 \end{Bmatrix} &= \begin{Bmatrix} \frac{\partial u_0}{\partial x} \\ \frac{\partial v_0}{\partial y} \\ \frac{\partial u_0}{\partial y} + \frac{\partial v_0}{\partial x} \end{Bmatrix}, \begin{Bmatrix} k_x^b \\ k_y^b \\ k_{xy}^b \end{Bmatrix} = \begin{Bmatrix} -\frac{\partial^2 w_b}{\partial x^2} \\ -\frac{\partial^2 w_b}{\partial y^2} \\ -2\frac{\partial^2 w_b}{\partial x \partial y} \end{Bmatrix}, \begin{Bmatrix} k_x^s \\ k_y^s \\ k_{xy}^s \end{Bmatrix} \\
 &= \begin{Bmatrix} -\frac{\partial^2 w_s}{\partial x^2} \\ -\frac{\partial^2 w_s}{\partial y^2} \\ -2\frac{\partial^2 w_s}{\partial x \partial y} \end{Bmatrix}, \\
 \begin{Bmatrix} \gamma_{yz}^0 \\ \gamma_{xz}^0 \end{Bmatrix} &= \begin{Bmatrix} \frac{\partial w_s}{\partial y} + \frac{\partial \varphi}{\partial y} \\ \frac{\partial w_s}{\partial x} + \frac{\partial \varphi}{\partial x} \end{Bmatrix}, \varepsilon_z^0 = \varphi
 \end{aligned}
 \tag{12}$$

The constitutive relations for the orthotropic state are as follows [6]:

$$\begin{Bmatrix} \sigma_x \\ \sigma_y \\ \sigma_z \\ \tau_{yz} \\ \tau_{xz} \\ \tau_{xy} \end{Bmatrix}^{(k)} = \begin{bmatrix} C_{11}^{(k)} & C_{12}^{(k)} & C_{13}^{(k)} & 0 & 0 & 0 \\ C_{12}^{(k)} & C_{22}^{(k)} & C_{23}^{(k)} & 0 & 0 & 0 \\ C_{13}^{(k)} & C_{23}^{(k)} & C_{33}^{(k)} & 0 & 0 & 0 \\ 0 & 0 & 0 & C_{44}^{(k)} & 0 & 0 \\ 0 & 0 & 0 & 0 & C_{55}^{(k)} & 0 \\ 0 & 0 & 0 & 0 & 0 & C_{66}^{(k)} \end{bmatrix} \begin{Bmatrix} \varepsilon_x \\ \varepsilon_y \\ \varepsilon_z \\ \gamma_{yz} \\ \gamma_{xz} \\ \gamma_{xy} \end{Bmatrix}
 \tag{13}$$

where in the above relation, σ_{ij} , ε_{ij} and C_{ij} are the stress, strain, and three-dimensional elastic constants, respectively. Moreover, index k ($= 1,3$) subscript represents the first to the third layer. The following equations provide the three-dimensional constants of elasticity:

$$\begin{aligned}
 C_{11}^{(k)} &= C_{22}^{(k)} = C_{33}^{(k)} = \frac{(1 - \nu^{(k)})}{\nu^{(k)}} \lambda^{(k)}, C_{12}^{(k)} = C_{13}^{(k)} = C_{23}^{(k)} = \lambda^{(k)} \\
 C_{44}^{(k)} &= C_{55}^{(k)} = C_{66}^{(k)} = G^{(k)} = \mu^{(k)} = \frac{E^{(k)}}{2(1 + \nu^{(k)})} \\
 C_{11}^{(2)} &= \frac{E_1^{(2)}}{1 - \nu_{12}^{(2)} \nu_{21}^{(2)}}, C_{22}^{(2)} = \frac{E_2^{(2)}}{1 - \nu_{12}^{(2)} \nu_{21}^{(2)}} \\
 C_{66}^{(2)} &= G_{12}^{(2)}, C_{44}^{(2)} = G_{23}^{(2)}, C_{55}^{(2)} = G_{13}^{(2)}, C_{12}^{(2)} = C_{21}^{(2)}
 \end{aligned}
 \tag{14}$$

where in the aforementioned relationship, the parameters are:

$$\lambda^{(k)} = \frac{\nu E^{(k)}}{(1 - 2\nu^{(k)})(1 + \nu^{(k)})}, \mu^{(k)} = G^{(k)} = \frac{E}{2(1 + \nu)}
 \tag{15}$$

2.3 Governing Equations

Hamilton’s principle for obtain the equations of motion is as follows [44]:

$$\int_0^t (\delta U + \delta K - \delta T) dt = 0
 \tag{16}$$

where δU , δK , and δT indicate variations in strain energy, potential energy, and kinetic energy, respectively.

Variations of the strain energy is computed as follows:

$$\begin{aligned}
 \delta U &= \int_V [\sigma_x \delta \varepsilon_x + \sigma_y \delta \varepsilon_y + \sigma_z \delta \varepsilon_z + \tau_{xy} \delta \gamma_{xy} + \tau_{yz} \delta \gamma_{yz} + \tau_{xz} \delta \gamma_{xz}] dV \\
 &= \int_A [N_x \delta \varepsilon_x^0 + N_y \delta \varepsilon_y^0 + N_z \delta \varepsilon_z^0 + N_{xy} \delta \gamma_{xy}^0 + M_x^b \delta k_x^b + M_y^b \delta k_y^b + M_{xy}^b \delta k_{xy}^b \\
 &\quad + M_x^s \delta k_x^s + M_y^s \delta k_y^s + M_{xy}^s \delta k_{xy}^s + S_{yz}^s \delta \gamma_{yz} + S_{xz}^s \delta \gamma_{xz}] dA
 \end{aligned}
 \tag{17}$$

where stress resultants N , M , and S in the aforementioned relationship are as follows:

$$\begin{aligned} \begin{Bmatrix} N_x & N_y & N_{xy} \\ M_x^b & M_y^b & M_{xy}^b \\ M_x^s & M_y^s & M_{xy}^s \end{Bmatrix} &= \sum_{n=1}^3 \int_{h_n}^{h_{n+1}} (\sigma_x, \sigma_y, \tau_{xy})^{(n)} \begin{Bmatrix} 1 \\ z \\ f \end{Bmatrix} dz \\ N_z &= \sum_{n=1}^3 \int_{h_n}^{h_{n+1}} (\sigma_z)^{(n)} g' dz \\ (S_{xz}^s, S_{yz}^s) &= \sum_{n=1}^3 \int_{h_n}^{h_{n+1}} (\tau_{xz}, \tau_{yz})^{(n)} g dz \end{aligned} \tag{18}$$

In the above relations, the parameters h_{n+1} and h_n are the locations of the top and bottom layers of the n th layer in z direction.

Variations of potential energy of applied loads are expressed in the following format:

$$\delta k = - \int_A q \delta(w_b + w_s + w_{st}) dA \tag{19}$$

In the aforementioned connection, q represents the concentrated transverse load.

Variations of the plate’s kinetic energy may be expressed as follows:

$$\begin{aligned} \delta T &= \int_V [\dot{u} \delta \dot{u} + \dot{v} \delta \dot{v} + \dot{w} \delta \dot{w}] \rho dV \\ &= \int_A \{ I_0(\dot{u}_0 \delta \dot{u}_0 + \dot{v}_0 \delta \dot{v}_0 + (\dot{w}_b + \dot{w}_s)(\delta \dot{w}_b + \delta \dot{w}_s)) \\ &\quad - I_1 \left(\dot{u}_0 \frac{\partial \delta \dot{w}_b}{\partial x} + \frac{\partial \dot{w}_b}{\partial x} \delta \dot{u}_0 + \dot{v}_0 \frac{\partial \delta \dot{w}_b}{\partial y} + \frac{\partial \dot{w}_b}{\partial y} \delta \dot{v}_0 \right) \\ &\quad - J_1 \left(\dot{u}_0 \frac{\partial \delta \dot{w}_s}{\partial x} + \frac{\partial \dot{w}_s}{\partial x} \delta \dot{u}_0 + \dot{v}_0 \frac{\partial \delta \dot{w}_s}{\partial y} + \frac{\partial \dot{w}_s}{\partial y} \delta \dot{v}_0 \right) \\ &\quad + I_2 \left(\frac{\partial \dot{w}_b}{\partial x} \frac{\partial \delta \dot{w}_b}{\partial x} + \frac{\partial \dot{w}_b}{\partial y} \frac{\partial \delta \dot{w}_b}{\partial y} \right) + K_2 \left(\frac{\partial \dot{w}_s}{\partial x} \frac{\partial \delta \dot{w}_s}{\partial x} + \frac{\partial \dot{w}_s}{\partial y} \frac{\partial \delta \dot{w}_s}{\partial y} \right) \\ &\quad + J_2 \left(\frac{\partial \dot{w}_b}{\partial x} \frac{\partial \delta \dot{w}_s}{\partial x} + \frac{\partial \dot{w}_s}{\partial x} \frac{\partial \delta \dot{w}_b}{\partial x} + \frac{\partial \dot{w}_b}{\partial y} \frac{\partial \delta \dot{w}_s}{\partial y} + \frac{\partial \dot{w}_s}{\partial y} \frac{\partial \delta \dot{w}_b}{\partial y} \right) \\ &\quad + J_1^s ((\dot{w}_b + \dot{w}_s) \delta \dot{\varphi} + \dot{\varphi} \delta (\dot{w}_b + \dot{w}_s)) + K_2^s \dot{\varphi} \delta \dot{\varphi} \} dA \end{aligned} \tag{20}$$

In the above relations, ρ represents the plate’s density, and:

$$\begin{aligned} (I_0, I_1, J_1, J_1^s, I_2, J_2, K_2, K_2^s) &= \sum_{n=1}^3 \int_{h_n}^{h_{n+1}} (1, z, f, g, z^2, zf, f^2, g^2) \rho dz \end{aligned} \tag{21}$$

After some mathematical efforts and some simplifications, final definition of five equations of motion is as follow:

$$\begin{aligned} \delta u_0 : & A_{11} d_{11} u_0 + A_{66} d_{22} u_0 + (A_{12} + A_{66}) d_{12} v_0 - B_{11} d_{11} w_b \\ & - (B_{12} + 2B_{66}) d_{12} w_b \end{aligned} \tag{22}$$

$$\begin{aligned} & - (B_{12}^s + 2B_{66}^s) d_{12} w_s - B_{11}^s d_{11} w_s + L d_1 \varphi \\ & = I_0 \ddot{u}_0 - I_1 d_1 \ddot{w}_b - J_1 d_1 \ddot{w}_s \end{aligned}$$

$$\begin{aligned} \delta v_0 : & A_{22} d_{22} v_0 + A_{66} d_{11} v_0 + (A_{12} + A_{66}) d_{12} u_0 - B_{22} d_{22} w_b \\ & - (B_{12} + 2B_{66}) d_{11} w_b \\ & - (B_{12}^s + 2B_{66}^s) d_{11} w_s - B_{22}^s d_{22} w_s + L d_2 \varphi \\ & = I_0 \ddot{v}_0 - I_1 d_2 \ddot{w}_b - J_1 d_2 \ddot{w}_s \end{aligned} \tag{23}$$

$$\begin{aligned} \delta w_b : & B_{11} d_{11} u_0 + (B_{12} + 2B_{66}) d_{12} u_0 + (B_{12} + 2B_{66}) d_{11} v_0 \\ & + B_{22} d_{22} v_0 \\ & - D_{11} d_{11} w_b - 2(D_{12} + 2D_{66}) d_{11} w_b \\ & - D_{22} d_{22} w_b - D_{11}^s d_{11} w_s \\ & - 2(D_{12}^s + 2D_{66}^s) d_{11} w_s - D_{22}^s d_{22} w_s \\ & + L^s (d_{11} \varphi + d_{22} \varphi) + q = I_0 (\ddot{w}_b + \ddot{w}_s) \\ & + I_1 (d_{11} \ddot{u}_0 + d_{22} \ddot{v}_0) - I_2 (d_{11} \ddot{w}_b + d_{22} \ddot{w}_b) \\ & - J_2 (d_{11} \ddot{w}_s + d_{22} \ddot{w}_s) + J_1^s \ddot{\varphi} \end{aligned} \tag{24}$$

$$\begin{aligned} \delta w_s : & B_{11}^s d_{11} u_0 + (B_{12}^s + 2B_{66}^s) d_{12} u_0 + (B_{12}^s + 2B_{66}^s) d_{11} v_0 \\ & + B_{22}^s d_{22} v_0 \\ & - D_{11}^s d_{11} w_b - 2(D_{12}^s + 2D_{66}^s) d_{11} w_b \\ & - D_{22}^s d_{22} w_b - H_{11}^s d_{11} w_s \\ & - 2(H_{12}^s + 2H_{66}^s) d_{11} w_s - H_{22}^s d_{22} w_s + A_{44}^s d_{11} w_s \\ & + A_{55}^s d_{22} w_s \\ & + R (d_{11} \varphi + d_{22} \varphi) + A_{44}^s d_{11} \varphi + A_{55}^s d_{22} \varphi + q \\ & = I_0 (\ddot{w}_b + \ddot{w}_s) \\ & + J_1 (d_{11} \ddot{u}_0 + d_{22} \ddot{v}_0) - J_2 (d_{11} \ddot{w}_b + d_{22} \ddot{w}_b) \\ & - K_2 (d_{11} \ddot{w}_s + d_{22} \ddot{w}_s) + J_1^s \ddot{\varphi} \end{aligned} \tag{25}$$

$$\begin{aligned} \delta \varphi : & L (d_{11} u_0 + d_{22} v_0) - L^s (d_{11} w_b + d_{22} w_b) + (R - A_{44}^s) d_{11} w_s \\ & + (R - A_{55}^s) d_{22} w_s \\ & + R^s \varphi - A_{44}^s d_{11} \varphi - A_{55}^s d_{22} \varphi = J_1^s (\ddot{w}_b + \ddot{w}_s) + K_2^s \ddot{\varphi} \end{aligned} \tag{26}$$

In the above relationships, d_{ij} , d_{ijl} , and d_{ijlm} are differential operators with the following definitions:

$$\begin{aligned} d_{ij} &= \frac{\partial^2}{\partial x_i \partial x_j}, \quad d_{ijl} = \frac{\partial^3}{\partial x_i \partial x_j \partial x_l}, \quad d_{ijlm} \\ &= \frac{\partial^4}{\partial x_i \partial x_j \partial x_l \partial x_m}, \quad (i, j, l, m = 1, 2) \end{aligned} \tag{27}$$

In addition:

$$\begin{Bmatrix} L \\ L^s \\ R \\ R^s \end{Bmatrix} = \sum_{n=1}^3 \int_{h_n}^{h_{n+1}} \lambda \begin{Bmatrix} 1 \\ z \\ f \\ g' \frac{1-v}{v} \end{Bmatrix} g' dz \tag{28}$$

In the equations of motion (21)-(26), the stiffness matrices are derived as follows:

$$\begin{Bmatrix} A_{11} & B_{11} & D_{11} & B_{11}^s & D_{11}^s & H_{11}^s \\ A_{12} & B_{12} & D_{12} & B_{12}^s & D_{12}^s & H_{12}^s \\ A_{66} & B_{66} & D_{66} & B_{66}^s & D_{66}^s & H_{66}^s \end{Bmatrix} = \sum_{n=1}^3 \int_{h_n}^{h_{n+1}} \lambda(1, z, z^2, f, zf, f^2) \begin{Bmatrix} \frac{1-v}{v} \\ 1 \\ \frac{1-2v}{2v} \end{Bmatrix} dz$$

$$(A_{22}, B_{22}, D_{22}, B_{22}^s, D_{22}^s, H_{22}^s) = (A_{11}, B_{11}, D_{11}, B_{11}^s, D_{11}^s, H_{11}^s)$$

$$A_{44}^s = A_{55}^s = \sum_{n=1}^3 \int_{h_n}^{h_{n+1}} \mu(g)^2 dz \tag{29}$$

2.4 Exact Solution

In the present study, the boundary conditions of the sandwich plate at the lateral edges are simple supports, and Navier’s technique may be employed in the space domain to discretize the differential equations of system. In order to satisfy the boundary conditions, the displacement field variables are addressed in the following double Fourier sinusoidal series form [24]:

$$\begin{Bmatrix} u_0 \\ v_0 \\ w_b \\ w_s \\ \varphi \end{Bmatrix} = \sum_{m=1}^{\infty} \sum_{n=1}^{\infty} \begin{Bmatrix} u(t) \cos(\alpha x) \sin(\beta y) \\ v(t) \sin(\alpha x) \cos(\beta y) \\ w_b(t) \sin(\alpha x) \sin(\beta y) \\ w_s(t) \sin(\alpha x) \sin(\beta y) \\ \varphi(t) \sin(\alpha x) \sin(\beta y) \end{Bmatrix} \tag{30}$$

In the following connection, $u(t)$, $v(t)$, $w_b(t)$, $w_s(t)$, and $\varphi(t)$ indicate the time parameters of the dynamic response and:

$$\alpha = m\pi/a \quad \beta = n\pi/b \tag{31}$$

where parameters a and b are the sheet’s length and width. Moreover, the transverse load q is expanded as follows in the double Fourier sinusoidal series:

$$q(x, y, t) = \sum_{m=1}^{\infty} \sum_{n=1}^{\infty} q_{mn} \sin(\alpha x) \sin(\beta y) \tag{32}$$

The term q_{mn} , which is considered to represent a concentrated load, will be discussed in the section on impact modeling.

By substituting Eqs. (30) into the equations of motion (22)-(26), the following differential equations are obtained from which we may determine the dynamic reaction of the sheet:

$$[M]\{\ddot{\chi}\} + [K]\{\chi\} = \{Q\} \tag{33}$$

$[M]$ and $[K]$ are the mass and stiffness matrices of the system, respectively, and $\{Q\}$ represents the impact force. The analytical solution to the above problem is obtained through the Newmark time integral solution method. The values of a_{ij} and m_{ij} are given in the appendix.

In addition, eigen-frequency associated with the (m,n) th mode is obtained from solution of following eigen-value problem:

$$\left(\begin{bmatrix} a_{11} & a_{12} & a_{13} & a_{14} & a_{15} \\ a_{12} & a_{22} & a_{23} & a_{24} & a_{25} \\ a_{13} & a_{23} & a_{33} & a_{34} & a_{35} \\ a_{14} & a_{24} & a_{34} & a_{44} & a_{45} \\ a_{15} & a_{25} & a_{35} & a_{45} & a_{55} \end{bmatrix} - \omega^2 \begin{bmatrix} m_{11} & 0 & m_{13} & m_{14} & 0 \\ 0 & m_{22} & m_{23} & m_{24} & 0 \\ m_{13} & m_{23} & m_{33} & m_{34} & m_{35} \\ m_{14} & m_{24} & m_{34} & m_{44} & m_{45} \\ 0 & 0 & m_{35} & m_{45} & m_{55} \end{bmatrix} \right) \begin{Bmatrix} U_{mn} \\ V_{mn} \\ W_{bmn} \\ W_{smn} \\ \Phi_{mn} \end{Bmatrix} = 0 \tag{34}$$

where U_{mn} , V_{mn} , W_{bmn} , W_{smn} , and Φ_{mn} are arbitrary parameters associated with (m,n) th eigen-vector mode.

3 Impact Modeling:

Two degrees of freedom of mass and spring model is used to calculate the impact force and the transverse deflection of the sheet at the point of impact [12, 45]. This vibration method is used when the boundary conditions are only applied to the surfaces, the surfaces and the middle core of the sheet are in the elastic area at the moment of impact, and the middle core of the sheet is not crushed. Figure 3 depicts the two-degree-of-freedom system under consideration.

In Fig. 3, M_{eff}^P represents the effective mass of the sandwich panel, m_I represents the projectile mass, K_c^* indicates the linearized contact stiffness, and K_g indicates the sandwich panel’s equivalent stiffness.

The impactor is assumed to impact the middle of the sandwich sheet with an initial velocity of V_0 . By using Newton’s second law, the following equations of motion may be derived

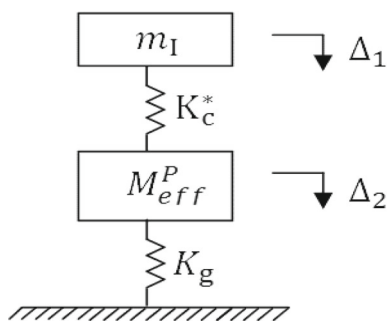


Fig. 3 Two-degree-of-freedom mass and spring configuration [12]

for two-degree-of-freedom system:

$$\begin{cases} m_I \ddot{\Delta}_1 + K_c^*(\Delta_1 - \Delta_2) = 0 \\ M_{eff}^P \ddot{\Delta}_2 + K_c^*(\Delta_2 - \Delta_1) + K_g \Delta_2 = 0 \end{cases} \quad (35)$$

The effective mass of the panel for the simple support mode is equal to one-fourth of the sandwich panel’s overall mass [12]. The relationship (36) describes the vertical displacement of the impacting mass and the effective mass of the sandwich panel.

$$\begin{aligned} \Delta_1 &= A_1 \sin(\omega t + \varphi) \\ \Delta_2 &= A_2 \sin(\omega t + \varphi) \end{aligned} \quad (36)$$

The equivalent stiffness at the impact point may be derived from the static analysis using the higher-order theory of sandwich sheets [12] and, in the special case when the impact occurs in the center of the surface, from the following relationship [11]:

$$K_g = M_{tot} \omega_{11}^2 \quad (37)$$

where ω_{11} is the frequency of the first mode of vibration, which is found using equation (34). The following equation will be used to get the value of the contact stiffness for the enhanced Hertz contact law.

$$K_c = \frac{4}{3} E R^{1/2} \quad (38)$$

In the preceding relationship, E and R represent the plate’s elasticity coefficient and radius of curvature, as follows:

$$\frac{1}{R} = \frac{1}{R_1} + \frac{1}{R_2}, \quad \frac{1}{E} = \frac{1 - \nu_{eff}^2}{E_{eff}} + \frac{1 - \nu_{imp}^2}{E_{imp}} \quad (39)$$

In the above connection, R_1 and R_2 represent the curvature of the impactor and the plate, respectively, while E_{imp} , ν_{imp} , E_{eff} , and ν_{eff} represent the effective elasticity and Poisson coefficients for the impactor and the plate, respectively.

Moreover:

$$\begin{aligned} E_{eff} &= \frac{h}{\frac{h_t}{E_{33t}} + \frac{h_b}{E_{33b}} + \frac{h_c}{E_{33c}}} \\ v_{eff} &= \nu_{13t} \left(\frac{h_t}{h} \right) + \nu_{13b} \left(\frac{h_b}{h} \right) + \nu_{13c} \left(\frac{h_c}{h} \right) \end{aligned} \quad (40)$$

By linearizing the relationship (38) about the maximum impact force and the maximum relative shape change between the impactor and the target, the following relationship can be expressed [11]:

$$K_c^* = K_c^n F_{max}^{\frac{n-1}{n}} \quad (41)$$

where K_c represents the enhanced Hertz contact stiffness and is determined by Eq. (38). The value of n is often 1.5. The maximum contact force may be determined using the concept of energy conservation by equating the initial kinetic energy of the impactor with the work done or the strain energy stored in the springs:

$$\frac{F_{max}^2}{2K_g} + \frac{F_{max}^{1+\frac{1}{n}}}{(n+1)K_c^{\frac{1}{n}}} = \frac{1}{2} m_I V_0^2 \quad (42)$$

By replacing the Eqs. (36) in the formula (35), and by sorting and converting to the matrix multiplication mode, it is obtained:

$$\begin{bmatrix} -m_I \omega^2 + K_c^* & -K_c^* \\ -K_c^* & -M_{eff}^P \omega^2 + K_c^* + K_g \end{bmatrix} \begin{bmatrix} A_1 \\ A_2 \end{bmatrix} = 0 \quad (43)$$

To solve the given system of equations, the determinants of the matrix of coefficients must be made equal to zero, resulting in:

$$(m_I M_{eff}^P \omega^4 + (-m_I K_c^* - m_I K_g - K_c^* M_{eff}^P) \omega^2 + K_c^* K_g = 0 \quad (44)$$

By solving the preceding equation, we get two values for ω_{n1} and ω_{n2} . We represent the values of elements of Eigen-vector A_1 associated with ω_{n1} as $A_1^{(1)}$, $A_2^{(1)}$ and elements of Eigen-vector A_2 associated with ω_{n2} as $A_1^{(2)}$, $A_2^{(2)}$. The ratios of $r_1 = \frac{A_2^{(1)}}{A_1^{(1)}}$ and $r_2 = \frac{A_2^{(2)}}{A_1^{(2)}}$ may be found given the values of ω_{n1} and ω_{n2} using the following relations:

$$r_1 = \frac{A_2^{(1)}}{A_1^{(1)}} = \frac{-m_I \omega_{n1}^2 + K_c^*}{K_c^*} = \frac{K_c^*}{-M_{eff}^P \omega_{n1}^2 + K_c^* + K_g} \quad (45)$$

$$r_2 = \frac{A_2^{(2)}}{A_1^{(2)}} = \frac{-m_I \omega_{n2}^2 + K_c^*}{K_c^*} = \frac{K_c^*}{-M_{eff}^p \omega_{n2}^2 + K_c^* + K_g} \quad (46)$$

The natural states of oscillatory motion associated with ω_{n1}^2 and ω_{n2}^2 may be described as relations (47), based on the ratios derived from relations (45) and (46).

$$\vec{\varphi}^{(1)} = \begin{Bmatrix} A_1^{(1)} \\ A_2^{(1)} \end{Bmatrix} = \begin{Bmatrix} A_1^{(1)} \\ r_1 A_1^{(1)} \end{Bmatrix} \vec{\varphi}^{(2)} = \begin{Bmatrix} A_1^{(2)} \\ A_2^{(2)} \end{Bmatrix} = \begin{Bmatrix} A_1^{(2)} \\ r_2 A_1^{(2)} \end{Bmatrix} \quad (47)$$

The system's overall motion at time t may be described as follows:

$$\begin{Bmatrix} \Delta_1 \\ \Delta_2 \end{Bmatrix} = C_1 \vec{\varphi}^{(1)} \sin(\omega_{n1}t + \psi_1) + C_2 \vec{\varphi}^{(2)} \sin(\omega_{n2}t + \psi_2) \quad (48)$$

The unknown coefficients C_1 , C_2 , ψ_1 , and ψ_2 may be found by applying the initial conditions listed below:

$$\begin{Bmatrix} \Delta_1(t=0) = 0 \\ \Delta_2(t=0) = 0 \end{Bmatrix}, \begin{Bmatrix} \dot{\Delta}_1(t=0) = V_0 \\ \dot{\Delta}_2(t=0) = 0 \end{Bmatrix} \quad (49)$$

We have, by applying the initial conditions:

$$\begin{aligned} \psi_1 &= \psi_2 = 0 \\ C_1 &= \frac{V_0 r_2}{\omega_{n1}(r_2 - r_1)} \quad C_2 = -\frac{r_1 \omega_{n1}}{r_2 \omega_{n2}} C_1 \end{aligned} \quad (50)$$

The contact force function may be determined by knowing the unknowns in Eq. (48):

$$F(t) = K_c^*(\Delta_1 - \Delta_2) \quad (51)$$

Applying the aforementioned relationship, the contact force history may be calculated. To compute the history of the sheet's deflection, we model the contact force function as a concentrated load at the sheet's center:

$$q_{mn} = \frac{4F(t)}{ab} \sin \frac{m\pi x_0}{a} \sin \frac{n\pi y_0}{b} \quad (52)$$

According to the equation presented, $x_0 = \frac{a}{2}$ and $y_0 = \frac{b}{2}$. Now, we insert Eq. (52) into Eq. (32) and solve Eq. (34) using Newmark's time integral to get the deflection history in the center of the sheet.

Table 1 Geometric characteristics of sandwich panel with auxetic core

a (m)	b (m)	h_{tot} (m)	h_c (m)
0.2	0.2	0.01	0.009

Table 2 Physical characteristics of aluminum sheet surfaces

E (GPa)	G (GPa)	ρ (kg/m ³)	ν
69	27	2700	0.3

4 Discussion and Results

In this section, the numerical findings' analysis is described. Before reviewing new results, we will confirm all the offered approaches, including the natural frequency of free vibration of the sandwich sheet, the two-degree-of-freedom mass and spring model, and the sheet's deflection based on the supplied theory. Lastly, we will compare the effects of the auxetic and non-auxetic cores on the impact response and investigate the parameters that influence the history of deflection and contact force of the sandwich sheet with the auxetic core.

The geometric specifications used for the sandwich panel with the auxetic core and aluminum face sheets are listed in Table 1. The physical properties of the aluminum top face sheets, the auxetic core, and the non-auxetic core are listed in Table 2 and 3. In addition, the specifications of the steel impactor with a steel spherical head are listed in Table 4.

4.1 Verification

4.1.1 Natural Frequency

To confirm the results, we first compare the fundamental frequency obtained from the HSNDT with those obtained from the study by Yuan et al. [47] for sandwich sheets with aluminum tops and honeycomb cores using finite element analysis. The material and geometric properties of the sandwich sheet used for the research by Yuan et al. are reported in Table 5, 6, 7 and the results of the two methods are listed in Table 8.

As Table 8 shows, the natural frequency found by the current method is very close to the natural frequency found by Yuan et al. [47]., which proves that the current method is accurate for finding the sheet's natural frequency.

4.1.2 Force's Time History and Impact Site's Deflection

To validate the accuracy of the two-degree-of-freedom mass and spring model, the force history of a steel ball hitting the center of a square steel sheet at a low speed with simple

Table 3 Physical properties of the auxetic and non-auxetic cores at various tilt angles [46]

θ	E_1 (GPa)	E_2 (GPa) ν_{12}	ν_{21}	G_{12} (GPa)	G_{23} (GPa)	G_{31} (GPa)	ρ (kg/m ³)
30°	0.1547	0.1547 – 0.9612	– 0.9612	0.0079	1.5588	1.7666	415.6921
45°	0.2403	0.0747 – 1.7240	– 0.5360	0.0097	1.4766	2.7086	590.6716
60°	0.5639	0.04043 – 3.5035	– 0.2511	0.0138	1.1905	4.7791	952.4022
– 30°	0.2578	0.0928 1.6019	0.5766	0.0079	0.9353	1.5588	249.4153

Table 4 Characteristics of the steel impactor with the steel spherical head

R (m)	m_I (kg)	E_{imp} (GPa)	ν_{imp}	V ($\frac{m}{s}$)
0.01	1.8	206	0.3	1

Table 5 Geometric characteristics of the sandwich sheet with honeycomb core [47]

a (mm)	b (mm)	h_t (mm)	h_b (mm)	h_c (mm)
1828.8	1219.2	0.4064	0.4064	6.35

Table 6 Material characteristics of the sandwich sheet tops with honeycomb core [47]

E (GPa)	ρ (kg/m ³)	G (GPa)	ν
68.948	2768	25.924	0.33

Table 7 Material properties of the honeycomb core [47]

E (GPa)	ρ (kg/m ³)	G_{yz} (GPa)	G_{zx} (GPa)	ν
0.3211	121.83	0.05171	0.13445	0.33

Table 8 Comparison between the fundamental frequency of the aluminum sandwich sheet with honeycomb core [47]

The present method	Yuan et al. [43]
23.45 (Hz)	23.41 (Hz)

Table 9 Material and geometrical characteristics of square steel sheet [48]

a (m)	b (m)	h (m)	E (GPa)	ρ (kg/m ³)	ν
0.2	0.2	0.008	206.8	7810	0.3

boundary conditions on all four sides is compared to the force history obtained by [48]. Material and geometric properties of the steel sheet are shown in Table 9; the steel ball has a radius of curvature of 10 mm and an initial velocity of 1 m/s.

According to Fig. 4, the results of the current approach in the mass and spring model and the theory utilized to derive

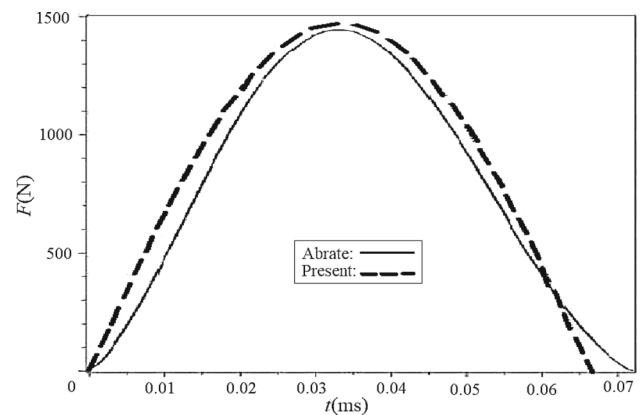


Fig. 4 A comparison of the temporal evolution of the impact force exerted on the simply supported plate by the steel sphere [48]

the time history of the impact force agree well with the results acquired from the reference.

In Fig. 5, time history of the plate’s deflection obtained by current research and those obtained by Shariyat et al. [49] are compared. The material and geometric properties of the sheet are shown in Table 10, and the steel ball has a radius of curvature of 10 mm and an initial velocity of 1 m/s. As can be observed, the outcome of this study is in excellent accord with that of Shariyat et al.

4.2 Effects of the Auxetic Core

As known, the auxetic materials are characterized by negative Poisson’s ratio. So, they have different behavior in bending compared to normal materials. To show this, we expose a monolayer auxetic core with simple support conditions to a static distributed load as shown and compare it with a normal

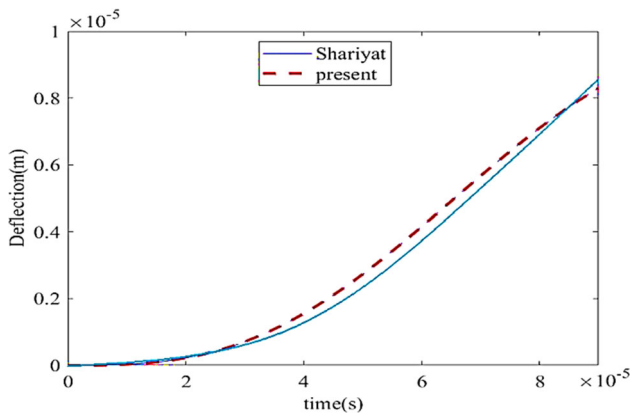


Fig. 5 A comparison between the present study by Shariyat et al. [49] regarding the time history of deflection due to low-velocity impact

Table 10 Material and geometrical features of rectangular steel sheet [49]

a (m)	b (m)	h (m)	E (GPa)	ρ (kg/m ³)	ν
0.5	0.4	0.002	206.8	7810	0.3

Table 11 Geometric properties of auxetic and honeycomb single-layer materials

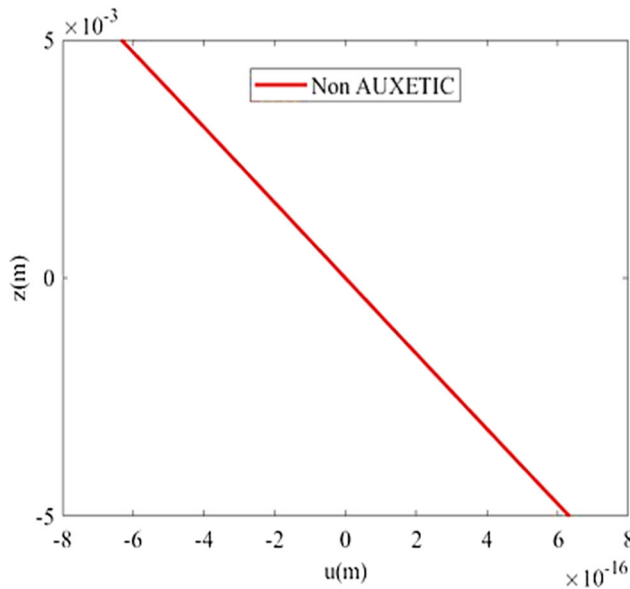
a (m)	b (m)	h (m)
0.2	0.2	0.01

regular honeycomb monolayer. The geometric characteristics of the single-layer sheet can be found in Table 11, and the material specifications of the auxetic and honeycomb core can be found in Table 3. Figure 6 displays the amount of displacement along the x-axis for the auxetic single layer and the ordinary honeycomb due to bending. As seen in the diagram, in contrast to the honeycomb core, the bending displacement of the auxetic core is inverted.

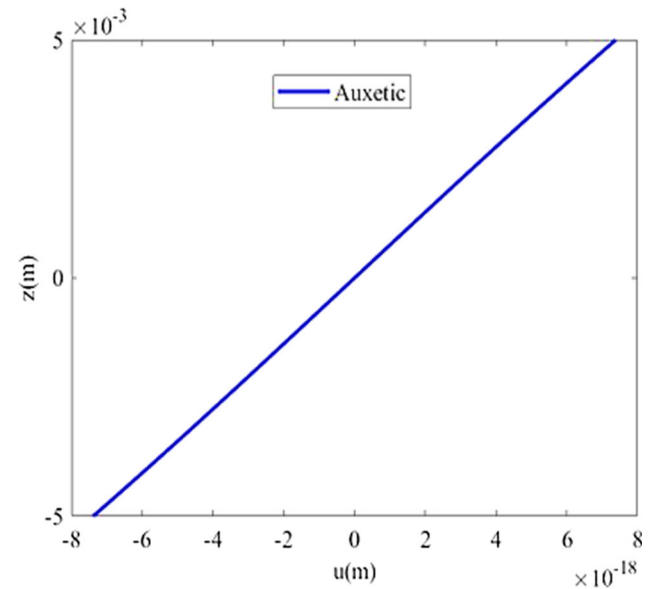
4.3 Numerical Results

In this section, the new numerical results analysis is described. This section’s objective is to examine the influence of various factors on the time histories of dynamic deflection and impact force in the ideal sandwich plate with auxetic core.

Figure 7 illustrates the time evolution of sandwich panel force for three different angles of inclination of the auxetic honeycomb cell. Evidently, the internal angle of the core has a major influence on the time history of the impact force. The smaller the angle of the auxetic cell, based on Eqs. (2), the transverse stiffer the auxetic core becomes. This enhancement of the core stiffness increases the ability to resist deformation of the struts. Consequently, when a sandwich panel experiences an impact force, a core with a larger angle of the auxetic cell will exhibit increased stiffness, thereby reducing deflection at the point of impact. As a result, the greater the cell’s degree of inclination, the longer the duration of impact and the lower the maximum impact



(a)



(b)

Fig. 6 Displacement in the x direction owing to the extensive load in the single layer of **a** normal and **b** auxetic honeycombs

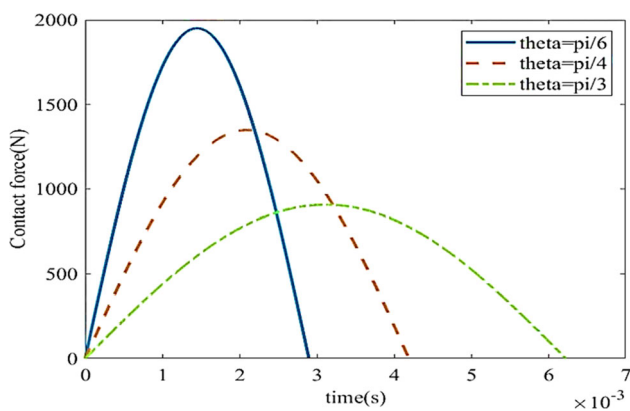


Fig. 7 Time history of impact force on the sandwich plate with different auxetic core internal angles

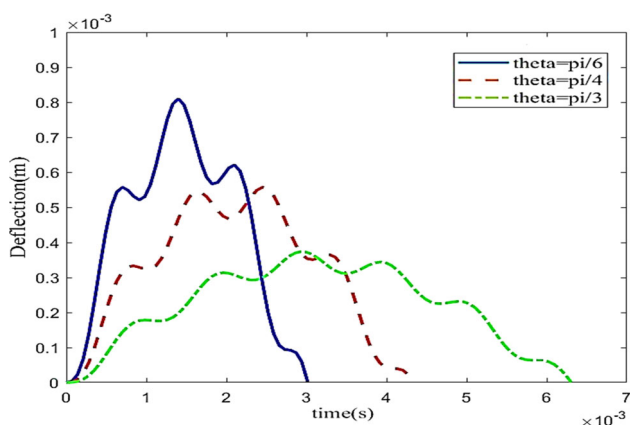


Fig. 8 Time history of the sandwich plate impact site deflection in auxetic cores with different internal angles

force. In addition, Fig. 8 shows the effect of the angle of inclination of the auxetic honeycomb cell on the time history of the impact site’s deflection. As can be observed, the larger angle of the auxetic cell causes a smaller deflection of the impact site. This is because raising the cellular slope of the auxetic core improves the elasticity coefficient, thereby increasing the sandwich panel’s stiffness and decreasing its deflection. Figure 8 indicates that the core with an internal angle of $\theta = 60^\circ$ is more effective in reducing the deflection amplitude.

Figures 9 and 10 compare the time histories of the impact force and impact site deflection for sandwich panels with auxetic and non-auxetic honeycomb cores, respectively. As shown in Fig. 9, the sandwich panel of the auxetic honeycomb has a longer collision time and a lower maximum contact force than the honeycomb panel with a positive Poisson ratio. Figure 10 demonstrates that the auxetic core deflects less than the non-auxetic core. The auxetic honeycomb core demonstrates a negative Poisson’s ratio, which implies that it expands sideways when subjected to longitudinal stretching.

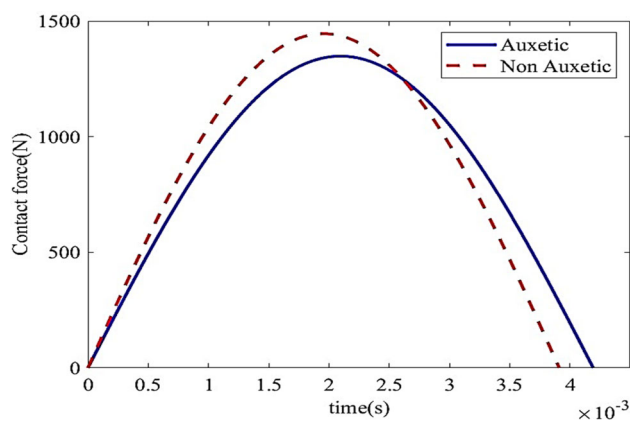


Fig. 9 Time history of the impact force of the sandwich panel with the auxetic honeycomb core at a 45° tilt angle and the non-auxetic honeycomb core at a -30° tilt angle

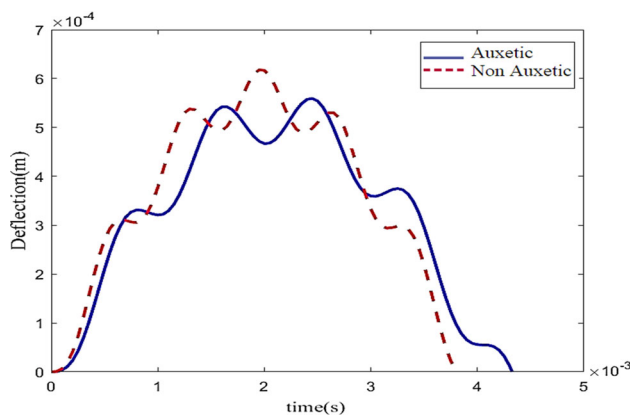


Fig. 10 History of the impact site deflection of the sandwich panel with the auxetic honeycomb core at a 45° tilt angle and the non-auxetic honeycomb core at a -30° tilt angle

This distinctive characteristic enables the core to efficiently absorb and distribute impact energy. In the event of a collision, the auxetic core undergoes controlled deformation, leading to an extended duration of the collision. Additionally, the expansion of the core aids in decreasing the maximum contact force by dispersing it across a wider surface area, thereby minimizing the occurrence of localized stress concentrations and potential damage.

In the following, we will continue with the material properties of auxetic honeycomb sandwich panel with 30° inclined angle.

Figure 11 illustrates time history of the impact force at various impact velocity. It can be observed, as the impactor’s velocity rises, so does the maximum impact force, but the duration of the impact reduces. These phenomena are a result of the impactor’s increased kinetic energy. A combination of an increase in the maximum impact force and a reduction in impact duration allows for a higher quantity of the impactor’s

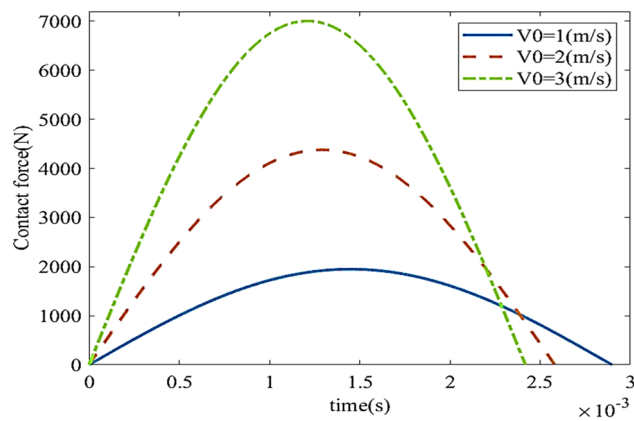


Fig. 11 Time history of impact force of the sandwich panel with the auxetic core for different speeds

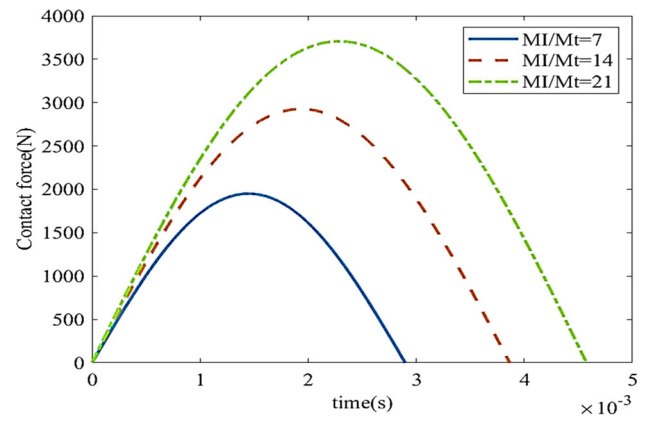


Fig. 13 Time history of the impact force of the sandwich panel with the auxetic core for different ratios of the impact mass to the total mass of the sheet

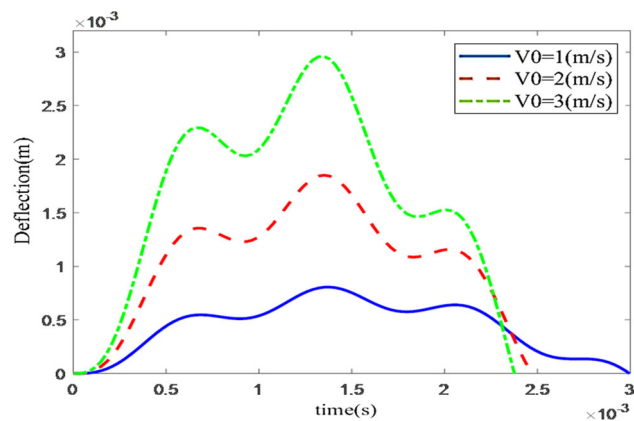


Fig. 12 Time history of deflection at the impact site of the sandwich panel with the auxetic core for different speeds

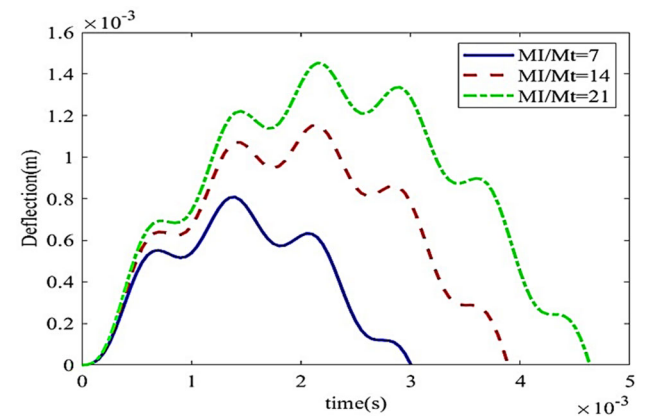


Fig. 14 Time history of deflection at the impact site of the sandwich panel with the auxetic core for different ratios of the impact mass to the total mass of the sheet

kinetic energy to transfer to the sandwich sheet with a shorter duration, which causes a shock to the structure.

Figure 12 depicts the time history of the deflection of the impact site for low-velocity impacts at various velocities. According to this graphic, as the impactor's velocity rises, so does the amount of deflection at the point of impact. The impact force is proportional to the rate of momentum change, which depends on the mass and velocity of the object causing the impact. When the velocity increases, both the rate of momentum change and the applied force increases correspondingly. The greater force exerted on the target material leads to a more pronounced deflection response.

Figures 13 and 14 illustrate the influence of the impacting mass on the time history of the impact force and the deflection of the impact site, respectively. The solution is found for various ratio of the impactor mass to the overall mass of the sheet; it is assumed that the total mass of the sheet to be around 0.256 kg. As seen from Fig. 13, when the mass of the impactor increases, both the maximum impact force and the duration of the impact increase. An increase in the impacting

mass increases the kinetic energy, which in turn raises the maximum force of the impact, resulting in an extension of the impact's duration. Also, Fig. 14 shows that as the impactor's mass goes up, so does its kinetic energy and, as a result, does the deflection at the impact site. This makes the duration of the impact longer.

Figure 15 depicts the time evolution of the impact force on the sandwich panel of the auxetic honeycomb for various ratios of the core thickness to the overall thickness. It is evident that the thicker core causes to the lighter mass of the sheet, reduces stiffness of the sheet, increases the maximum contact force and minimizes contact duration. In addition, Fig. 16 illustrates the time history of the deflection under low-velocity impact force for various ratios of core thickness to total thickness (h_c/h). According to this diagram, it is evident that the greater the core thickness, the greater the range of lateral displacements under the same load. Since the sandwich plate's overall thickness is constant, when the ratio of core thickness to total thickness (h_c/h) increases, the

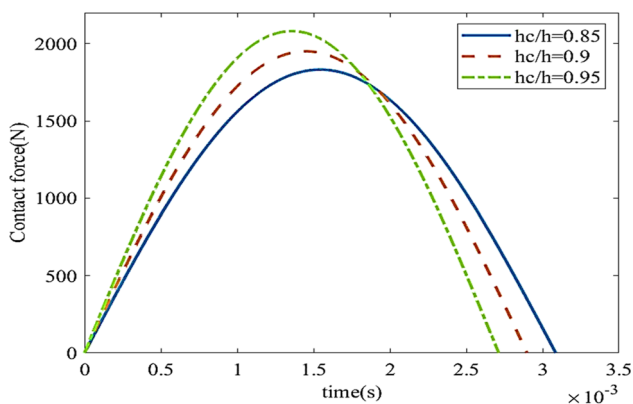


Fig. 15 Time history of the impact force of the sandwich panel with the auxetic core for different ratios of the core thickness to the total thickness

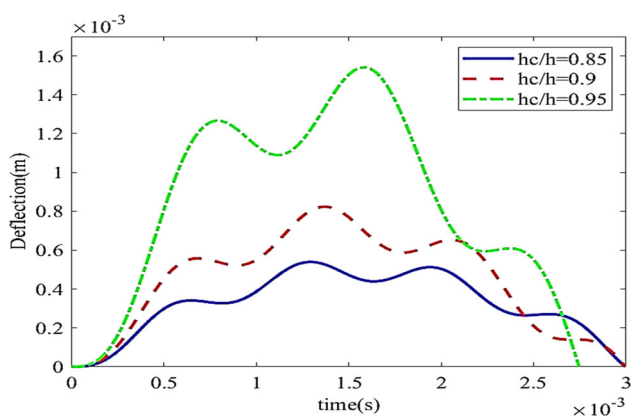


Fig. 16 Time history of deflection at the impact site of the sandwich panel with the auxetic core for different ratios of the core thickness to the total thickness

face sheet thickness decreases. This leads to a decrease in the flexural stiffness of the sandwich plate, an increase in the maximum deflection at the collision site, and a subsequent reduction in the collision duration.

5 Conclusion

In the current research, the time history of the impact force and the history of the impact site’s deflection caused by a low-velocity impact on a sandwich panel with the auxetic core were investigated. The effect of auxetic core and other geometrical parameters on the dynamic response of the sheet and the time history of impact force was explored. The low-velocity impact was modeled using the two-degree-of-freedom spring and mass model. Using Hamilton’s principle, the equations governing the dynamic response of the system were derived. In order to solve partial differential governing equations taking into account the boundary conditions

of simple supports, the analytical approach of Navier was utilized in the space domain and the numerical solution of Newmark was used in the time domain. The outcomes of this investigation are briefly discussed in the following section:

The results obtained from the two-degree-of-freedom mass and spring model and the high-order shear and normal deformation theory used in this study to determine the dynamic response and time history of the impact force are in excellent agreement with those of prior studies.

The auxetic honeycomb sandwich panel outperforms the non-auxetic honeycomb sandwich panel by 9.5% in minimizing deflection.

When the impactor’s velocity rises, the maximum impact force increases, the impact duration reduces, and the impact point’s deflection increases.

An increase in the impactor’s mass increases the kinetic energy and, thus, the maximum force; this, in turn, increases the collision’s duration and the deflection of the impact site.

The greater the thickness of the core, the greater the maximum contact force and the shorter the duration of the impact. Due to the lighter mass of the sheet, the equivalent stiffness of the sheet decreases, causing an increase in the maximum contact force, a decrease in the duration of the impact, and an increase in the deflection of the impact site.

The greater the angle of tilt of the auxetic core cell, the longer the duration of the impact, and the smaller the maximum time history of the contact force and deflection of the impact site; thus, the auxetic core with an angle of 60° has 54.73 percent less deflection than the core with an angle of 30°.

Appendix

The following terms apply to the matrix terms of Eq. (33).

$$\begin{aligned}
 a_{11} &= -(A_{11}\alpha^2 + A_{66}\beta^2), \quad a_{12} = -\alpha\mu(A_{12} + A_{66}) \\
 a_{13} &= \alpha[B_{11}\alpha^2 + (B_{12} + 2B_{66})\beta^2], \quad a_{14} = \alpha[B_{11}^s\alpha^2 + (B_{12}^s + 2B_{66}^s)\beta^2] \\
 a_{15} &= L\alpha, \quad a_{22} = -(A_{66}\alpha^2 + A_{22}\beta^2) \\
 a_{23} &= \beta[(B_{12} + 2B_{66})\alpha^2 + B_{22}\beta^2], \quad a_{24} = \beta[(B_{12}^s + 2B_{66}^s)\alpha^2 + B_{22}^s\beta^2] \\
 a_{25} &= L\beta, \quad a_{33} = -(D_{11}\alpha^4 + 2(D_{12} + 2D_{66})\alpha^2\beta^2 + D_{22}\beta^4) \\
 a_{34} &= -(D_{11}^s\alpha^4 + 2(D_{12}^s + 2D_{66}^s)\alpha^2\beta^2 + D_{22}^s\beta^4) \\
 a_{35} &= -L^s(\alpha^2 + \beta^2), \quad a_{44} \\
 &= -(H_{11}^s\alpha^4 + 2(H_{12}^s + 2H_{66}^s)\alpha^2\beta^2 + H_{22}^s\beta^4) + A_{55}^s\alpha^2 + A_{44}^s\beta^2 \\
 a_{45} &= \\
 &= -[A_{55}^s\alpha^2 + A_{44}^s\beta^2 + R(\alpha^2 + \beta^2)], \quad a_{55} = \\
 &= -(A_{44}^s\alpha^2 + A_{55}^s\beta^2 + R^s) \\
 m_{11} &= m_{12} = \\
 &= -I_0, \quad m_{13} = \alpha I_1, \quad m_{14} = \alpha J_1, \quad m_{23} = \beta I_1, \quad m_{24} = \beta J_1
 \end{aligned}$$

References

- Teymouri, H.; Biglari, H.: Elastodynamic green's functions for sandwich panels with aluminum foam core and transversely isotropic face sheets using potential functions method. *Eng. Anal. Bound. Elem.* **160**, 258–272 (2024)
- Jonas, P.; Kassapoglou, C.; Jonas, P.J.: Compressive strength of composite sandwich panels after impact damage: an experimental and analytical study. *J. Compos. Tech. Res.* **10**, 65–73 (1988)
- Olsson R.: Simplified theory for contact indentation of sandwich panels. Massachusetts Institute of Technology, Massachusetts (1994).
- Stephen, C.; Shivamurthy, B.; Mohan, M.; Mourad, A.-H.I.; Selvam, R.; Thimmappa, B.H.S.: Low velocity impact behavior of fabric reinforced polymer composites—a review. *Eng. Sci.* **18**, 75–97 (2022)
- Johnson, K.L.: Contact mechanics. Cambridge University Press, United States (1987)
- Mittal, R.K.; Khalili, M.R.: Analysis of impact of a moving body on an orthotropic elastic plate. *AIAA J.* **32**(4), 850–856 (1994)
- Huo, X.; Liu, H.; Luo, Q.; Sun, G.; Li, Q.: On low-velocity impact response of foam-core sandwich panels. *Int. J. Mech. Sci.* **181**, 105681 (2020)
- Guo, H.; Yuan, H.; Zhang, J.; Ruan, D.: Review of sandwich structures under impact loadings: experimental, numerical and theoretical analysis. *Thin-Walled Struct.* **196**, 111541 (2024)
- Lal, K.M.: Low velocity transverse impact behavior of 8-ply, graphite-epoxy laminates. *J. Reinf. Plast. Compos.* **2**(4), 216–225 (1983)
- Khalili, M.R.; Mittal, R.K.: Analysis of the dynamic response of large orthotropic elastic plates to transverse impact and its application to fibre-reinforced plates. Department of applied mechanics Indian institute of technology, Delhi (1992)
- Malekzadeh, K.; Khalili, M.R.; Mittal, R.K.: Response of composite sandwich panels with transversely flexible core to low-velocity transverse impact: a new dynamic model. *Int. J. Impact Eng* **34**(3), 522–543 (2007)
- Khalili, M.R.; Malekzadeh, K.; Mittal, R.K.: Effect of physical and geometrical parameters on transverse low-velocity impact response of sandwich panels with a transversely flexible core. *Compos. Struct.* **77**(4), 430–443 (2007)
- Tofighi, M.B.; Biglari, H.: FEM analyses of low velocity impact response of sandwich composites with nanoreinforced polypropylene core and alu-minum face sheets. *Phys. Mesomech.* **24**, 107–116 (2021)
- Tofighi, M.B.; Biglari, H.; Shokrieh, M.M.: An experimental and numerical investigation on the low-velocity impact response of nanoreinforced polypropylene core sandwich structures. *Mech. Compos. Mater.* **58**(2), 209–226 (2022)
- Lv, X.; Xiao, Z.; Fang, J.; Li, Q.; Lei, F.; Sun, G.: On safety vehicle for protection of vulnerable road users: a review. *Thin-Walled Struct.* **182**, 109990 (2023)
- Wang E.; Yao R.; Li Q.; Hu X.; Sun G.: Lightweight metallic cellular materials: A systematic review on mechanical characteristics and engineering applications. *Int. J. Mech. Sci.* 108795 (2023). <https://www.sciencedirect.com/science/article/abs/pii/S00207403230006975>
- Usta, F.; Türkmen, H.S.; Scarpa, F.: Low-velocity impact resistance of composite sandwich panels with various types of auxetic and non-auxetic core structures. *Thin-Walled Struct.* **163**, 107738 (2021)
- Lakes, R.: Foam structures with a negative Poisson's ratio. *Science* **235**(4792), 1038–1040 (1987)
- Wan, H.; Ohtaki, H.; Kotosaka, S.; Hu, G.: A study of negative Poisson's ratios in auxetic honeycombs based on a large deflection model. *Eur. J. Mech. - A/Solids.* **23**(1), 95–106 (2004)
- Zhang, X.-C.; An, L.-Q.; Ding, H.-M.; Zhu, X.-Y.; El-Rich, M.: The influence of cell micro-structure on the in-plane dynamic crushing of honeycombs with negative Poisson's ratio. *J. Sandw. Struct. Mater.* **17**(1), 26–55 (2014)
- Huang, J.; Zhang, Q.; Scarpa, F.; Liu, Y.; Leng, J.: In-plane elasticity of a novel auxetic honeycomb design. *Compos. Part B Eng.* **110**, 72–82 (2017)
- Prawoto, Y.: Seeing auxetic materials from the mechanics point of view: a structural review on the the negative poisson' ratio. *Comput. Mater. Sci.* **58**, 140–153 (2012)
- Qin, Q.; Xia, Y.; Li, J.; Chen, S.; Zhang, W.; Li, K.; Zhang, J.: On dynamic crushing behavior of honeycomb-like hierarchical structures with perforated walls: experimental and numerical investigations. *Int. J. Impact Eng* **145**, 103674 (2020)
- Reddy, J.N.: Mechanics of laminated composite plates and shells: theory and analysis. CRC Press, United States (2003)
- Khalili, M.R.; Malekzadeh, K.; Mittal, R.K.: A new approach to static and dynamic analysis of composite plates with different boundary conditions. *Compos. Struct.* **69**(2), 149–155 (2005)
- Zhang, J.; Ye, Y.; Qin, Q.; Wang, T.: Low-velocity impact of sandwich beams with fibre-metal laminate face-sheets. *Compos. Sci. Technol.* **168**, 152–159 (2018)
- Frostig, Y.; Baruch, M.; Vilnay, O.; Sheinman, I.: High-order theory for sandwich-beam behavior with transversely flexible core. *J. Eng. Mech.* **118**(5), 1026–1043 (1992)
- Malekzadeh, K.; Khalili, M.R.; Mittal, R.K.: Local and global damped vibrations of plates with a viscoelastic soft flexible core: an improved high-order approach. *J. Sandw. Struct. Mater.* **7**(5), 431–456 (2005)
- Zhang, J.; Qin, Q.; Zhang, J.; Yuan, H.; Du, J.; Li, H.: Low-velocity impact on square sandwich plates with fibre-metal laminate face-sheets: analytical and numerical research. *Compos. Struct.* **259**, 113461 (2021)
- Zhang, J.; Qin, Q.; Chen, S.; Yang, Y.; Ye, Y.; Xiang, C.; Wang, T.: Lowvelocity impact of multilayer sandwich beams with metal foam cores analytical, experimental, and numerical investigations. *J. Sandw. Struct. Mater.* **22**(3), 626–657 (2020)
- Yang, S.; Qi, C.; Wang, D.; Gao, R.; Hu, H.; Shu, J.: A comparative study of ballistic resistance of sandwich panels with aluminum foam and auxetic honeycomb cores. *Adv. Mech. Eng.* **5**, 589216 (2013)
- Allen, T.; Shepherd, J.; Hewage, T.A.M.; Senior, T.; Foster, L.; Alderson, A.: Low-kinetic energy impact response of auxetic and conventional open-cell polyurethane foams. *Phys. Stat. Solidi* **252**(7), 1631–1639 (2015)
- Qi, C.; Remennikov, A.; Pei, L.-Z.; Yang, S.; Yu, Z.-H.; Ngo, T.D.: Impact and close-in blast response of auxetic honeycomb-cored sandwich panels: experimental tests and numerical simulations. *Compos. Struct.* **180**, 161–178s (2017)
- Beharic, A.; Egui, R.R.; Yang, L.: Drop-weight impact characteristics of additively manufactured sandwich structures with different cellular designs. *Mater. Des.* **145**, 122–134 (2018)
- Hou, S.; Li, T.; Jia, Z.; Wang, L.: Mechanical properties of sandwich composites with 3d-printed auxetic and non-auxetic lattice cores under low velocity impact. *Mater. Des.* **160**, 1305–1321 (2018)
- Li, C.; Shen, H.-S.; Yang, J.; Wang, H.: Low-velocity impact response of sandwich plates with GRC face sheets and FG auxetic 3D lattice cores. *Eng. Anal. Bound. Elem.* **132**, 335–344 (2021)
- Qin, Q.; Chen, S.; Li, K.; Jiang, M.; Cui, T.; Zhang, J.: Structural impact damage of metal honeycomb sandwich plates. *Compos. Struct.* **252**, 112719 (2020)



38. Salami, S.J.: Dynamic extended high order sandwich panel theory for transient response of sandwich beams with carbon nanotube reinforced face sheets. *Aerosp. Sci. Technol.* **56**, 56–69 (2016)
39. Salami, S.J.: Low velocity impact response of sandwich beams with soft cores and carbon nanotube reinforced face sheets based on extended high order sandwich panel theory. *Aerosp. Sci. Technol.* **66**, 165–176 (2017)
40. Rekatsinas, C.S.; Siorikis, D.K.; Christoforou, A.P.; Chrysochoidis, N.A.; Saravanos, D.A.: Analysis of low velocity impacts on sandwich composite plates using cubic spline layerwise theory and semi empirical contact law. *Compos. Struct.* **194**, 158–169 (2018)
41. Zhang, J.; Zhu, X.; Yang, X.; Zhang, W.: Transient nonlinear responses of an auxetic honeycomb sandwich plate under impact loads. *Int. J. Impact Eng* **134**, 103383 (2019)
42. Zhu, X.; Zhang, J.; Zhang, W.; Chen, J.: Vibration frequencies and energies of an auxetic honeycomb sandwich plate. *Mech. Adv. Mater. Struct.* **26**(23), 1951–1957 (2019)
43. Bessaim, A.; Houari, M.S.A.; Tounsi, A.; Mahmoud, S.R.; Bedia, E.A.A.: A new higher-order shear and normal deformation theory for the static and free vibration analysis of sandwich plates with functionally graded isotropic face sheets. *J. Sandw. Struct. Mater.* **15**(6), 671–703 (2013)
44. Chen, D.; Yang, J.; Kitipornchai, S.: Free and forced vibrations of shear deformable functionally graded porous beams. *Int. J. Mech. Sci.* **108–109**, 14–22 (2016)
45. Malekzadeh Fard, K.; Payganeh, G.; Kardan, M.: Dynamic Response of Sandwich Panels with Flexible Cores and Elastic Foundation Subjected to Low-Velocity Impact. *Amirkabir J. Mech. Eng.* **45**(2), 27–42s (2013)
46. Choi, I.H.; Lim, C.H.: Low-velocity impact analysis of composite laminates using linearized contact law. *Compos. Struct.* **66**(1–4), 125–132 (2004)
47. Yuan, W.X.; Dawe, D.J.: Free vibration of sandwich plates with laminated faces. *Int. J. Numer. Methods Eng.* **54**(2), 195–217s (2002)
48. Abrate, S.: *Impact engineering of composite structures*. Springer Vienna, Austria (2011)
49. Shariyat, M.; Farzan, F.: Nonlinear eccentric low-velocity impact analysis of a highly prestressed FGM rectangular plate, using a refined contact law. *Arch. Appl. Mech.* **83**, 623–641 (2013)

Springer Nature or its licensor (e.g. a society or other partner) holds exclusive rights to this article under a publishing agreement with the author(s) or other rightsholder(s); author self-archiving of the accepted manuscript version of this article is solely governed by the terms of such publishing agreement and applicable law.

